A cerium-based metal-organic framework as adsorbent for the $^{99}Mo/^{99m}Tc$ generator

Ma, Chao; Wolterbeek, Hubert T.; Denkova, Antonia G.; Serra Crespo, Pablo

DOI
10.1016/j.seppur.2022.121218

Publication date
2022

Document Version
Final published version

Published in
Separation and Purification Technology

Separation and Purification Technology 295 (2022) 121218

Contents lists available at ScienceDirect

Separation and Purification Technology

journal homepage: www.elsevier.com/locate/seppur

A cerium-based metal-organic framework as adsorbent for the $^{99}Mo/^{99m}Tc$ generator

Chao Ma, Hubert T. Wolterbeek, Antonia G. Denkova *, Pablo Serra Crespo *

Applied radiation and isotopes, Radiation Science and Technology, Faculty of applied sciences, Delft University of Technology, 2629 JB Delft, Mekelweg 15, the Netherlands

ARTICLE INFO

Keywords:
UiO-66 (Ce)
Molybdenum
Adsorption mechanism
$^{99}Mo/^{99m}Tc$ generator

ABSTRACT

The cerium-based metal–organic framework UiO-66 (Ce) was examined as a potential adsorbent for the $^{99}Mo/^{99m}Tc$ generator. The results showed that the adsorbent had an outstanding adsorption performance, reaching up to 475 mg/g adsorption capacity at pH 3. An adsorption mechanism was proposed, where the adsorption was governed by hydrogen bonds, Ce-O-Mo coordination, π-anions and electrostatic interaction. Additionally, the adsorbent exhibited excellent radiation stability and good adsorption performance when radioactive ^{99}Mo was applied. A $^{99}Mo/^{99m}Tc$ generator was fabricated with UiO-66 (Ce) as adsorbent and its performance was evaluated over two weeks. The elution results showed that 92 ± 3% of ^{99m}Tc elution efficiency could be obtained with negligible cerium breakthrough, showing the great potential of UiO-66 (Ce) as adsorbent for $^{99}Mo/^{99m}Tc$ generators.

1. Introduction

Technetium-99 m, which is typically produced from the $^{99}Mo/^{99m}Tc$ generator, is the most applied diagnostic radionuclide in nuclear medicine [1]. Technetium-99 m, which is the decay product of molybdenum-99, can be separated from its parent radionuclide using various methods, for example, column chromatography, solvent extraction, sublimation and electrochemical separation [2]. Chromatographic separation is the most often applied due to its high efficiency, simplicity and speed of operation. When preparing commercial generators, ^{99}Mo is obtained as a ^{235}U fission product with high specific activity, which is essential due to the limited molybdenum adsorption capacity of the alumina adsorbent used (2 ~ 20 mg/g) in the commercial generators [3].

Alternative ^{99}Mo production routes involving the irradiation of molybdenum targets by the ^{98}Mo (n, γ) ^{99}Mo and the ^{100}Mo (γ, n) ^{99}Mo reactions have received attention in the last few years [4]. These processes have advantages such as lower cost, no nuclear waste and availability of many production places worldwide, i.e. nuclear research reactors and accelerators [5]. However, these routes produce low specific activity ^{99}Mo, what restricts its application using conventional alumina-based chromatography columns. To overcome this drawback, many adsorbents have been prepared and their performance in $^{99}Mo/^{99m}Tc$ generators has been explored. For example, Saptiama et al. synthesized mesoporous alumina under high calcination temperature, achieving maximum molybdenum adsorption of 41.6 mg/g [6]. The ^{99}Mo adsorption capacity of polymer zirconium composites synthesized by Tanase et al. could reach about 200 mg/g with ^{99m}Tc elution yield of 80% [7]. Chakravarty et al. developed some nanomaterials with an acceptable adsorption capacity from 70 to 250 mg/g, such as nano titania, nanocrystalline alumina and nano zirconia [8,9]. These materials, however, have limited molybdenum adsorption capacity due to their low surface area. Therefore, new adsorbents having higher adsorption capacity and fast uptake are still required.

Over the past few years, metal–organic frameworks (MOFs) have been extensively researched for diverse applications, due to their high surface area, easy functionalization and tuneable pore size [10,11]. One of the most studied MOFs is UiO-66 (University of Oslo), thanks to its outstanding thermal, chemical and mechanical stability [12,13]. Our previous work proved that UiO-66 (Zr) shows good performance and can be applied as an adsorbent for $^{99}Mo/^{99m}Tc$ generator [14]. Meanwhile, it was reported that cerium was a promising metal to use for MOF fabrication due to its inherent conversion trend between Ce^{4+} and Ce^{3+}, which could result in different adsorption sites [15]. The first cerium-based MOF with the UiO-66 structure was reported by Lammert., et al in 2015 [16] and was applied in various fields, including gas separation, catalysis and sensor [17–19].

* Corresponding authors.
E-mail addresses: A.G.Denkova@tudelft.nl (A.G. Denkova), P.SerraCrespo@tudelft.nl (P. Serra Crespo).

https://doi.org/10.1016/j.seppur.2022.121218
Received 24 March 2022; Received in revised form 27 April 2022; Accepted 2 May 2022
Available online 9 May 2022

In this study, the potential of UiO-66 (Ce) as a molybdenum adsorbent for $^{99}Mo/^{99m}Tc$ generator was explored. The molybdenum adsorption performance of UiO-66 (Ce), including adsorption kinetics and isotherms, was investigated by varying the molybdenum concentration and the pH value. The interaction between adsorbent and molybdenum species was also analysed by a combination of different characterization techniques, including zeta potential, Raman spectroscopy and X-ray photoelectron spectroscopy. The radiation stability of UiO-66 (Ce) was also investigated under gamma radiation. Furthermore, a $^{99}Mo/^{99m}Tc$ generator was fabricated with UiO-66 (Ce) and its performance was investigated including elution yield, ^{99}Mo breakthrough and cerium breakthrough.

2. Experimental section

2.1. Materials

1,4-benzenedicarboxylate (BDC, 98%), ammonium cerium(IV) nitrate ($(NH_4)_2Ce(NO_3)_6$, greater than95.5%) and N,N-dimethylformamide (DMF, 99.8%) were purchased from Sigma Aldrich. Molybdenum oxide ($\geq$ 99.95%) was purchased from Alfa Aesar. All chemical reagents were used without any purification.

2.2. Synthesis of Ce-based MOF

UiO-66 (Ce) was synthesized based on previously reported literature [16]. First, 1,4-benzenedicarboxylate (85.2 mmol) was dissolved into a glass bottle containing DMF (4.8 mL). Then, the aqueous solution of cerium ammonium nitrate (0.5333 M, 0.8 mL) was added to the mixture and the glass bottle was heated at 100 °C for 20 min using magnetic stirring. Afterwards, the precipitate was washed two times with DMF and ethanol, respectively. The obtained powder was dried at 70 °C for 12 h.

2.3. Characterization

The X-ray diffraction patterns of prepared MOF were recorded by a PANalytical X'pert Pro PW3040/60 diffractometer with Cu Kα radiation with an angular 2θ ranging from 5 ~ 40°. The surface area of the samples was determined by nitrogen adsorption at liquid nitrogen temperature by a Micromeritics Tristar II and calculated using the Brunauer-Emmett-Teller (BET) method. Inductively coupled plasma optical emission spectrometry (ICP-OES, Optima 4300 DV, Perkin Elmer) was applied to determine the molybdenum concentration before and after adsorption. The Zeta potential of the samples was performed within a pH range of 2 ~ 12 using a Malvern Zetasizer Nano S at room temperature. X-ray photoelectron spectra (XPS) were obtained on Thermofisher Scientific electron spectroscopy with Mg K-alpha source. The optical absorption property of sample was collected by a UV adsorption spectrophotometer (UV-6300PCC, VWR). The morphology and elements distribution of the adsorbent were studied using scanning electron microscopy (SEM, JEOL ISM-IT100) and energy dispersive spectroscopy (EDS, JEOL ISM-IT100). Raman spectroscopy of the sample was performed by a Raman spectrometer (LabRAM HR, HORIBA Scientific) with a green laser ($\lambda = 532$ nm) at room temperature. The prepared sample was irradiated by a Co-60 source with different doses (100 kGy, 350 kGy and 550 kGy) at a dose rate of 0.53 kGy/h.

2.4. Molybdenum adsorption

The effect of pH on the molybdenum adsorption uptake of UiO-66 (Ce) was studied for a pH range of 2 ~ 12. Typically, 6 mg of the adsorbent was added to Eppendorf tubes with different molybdenum concentrations (0.1 ~ 20 mg/mL). All tubes were shaken for 20 h at room temperature by a temperature-controlled vibrator. Then, the adsorbents were separated using a centrifuge and the supernatant solution was diluted at appropriate times for concentration measurement using ICP-OES. The uptake (q) was defined by the following equation:

$$q=(C_b\text{-}C_a)*V/m$$

Where C_b and C_a (mg/mL) are the molybdenum concentration before and after adsorption, respectively. V (mL) and m (mg) represent the volume of molybdenum solution and mass of adsorbent, respectively. All adsorption experiments were performed in triplicate. The details about column preparation of the $^{99}Mo/^{99m}Tc$ generator and the separation of radionuclides were described in Supporting Information S-1.

3. Results and discussion

3.1. Characterization

The morphology and elemental distribution of UiO-66 (Ce) were determined by SEM and EDS. As shown in Fig. 1, it can be observed that the prepared sample had spherical particles with a diameter of around 400 nm. The EDS mapping showed the presence of uniformly distributed C, O, Ce. Fig. 2 (a) shows the XRD patterns of UiO-66 (Ce) before and after molybdenum adsorption. The pattern of UiO-66 (Ce) prior to molybdenum adsorption displayed all diffractions peaks consistent with the simulated XRD pattern (also shown in Fig. 2 (a)) and no impurities were observed. Fig. 2 (b) displays the N_2 adsorption–desorption isotherms of UiO-66 (Ce) at 77 K. The adsorption isotherms belong to the type I adsorption curve. The calculated BET surface area and micropore volumes were 1140 m^2/g and 0.4 cm^3/g, respectively. The XRD and N_2 adsorption results of UiO-66 (Ce) after molybdenum adsorption in Fig. 2 will be discussed later.

3.2. Molybdenum adsorption studies

3.2.1. Effect of pH

The pH of the solution influences the formation of molybdenum species and therefore its effect on the molybdenum adsorption was investigated [20]. Fig. 3 (a) shows the zeta potential of UiO-66 (Ce) and its isoelectric point (IEP) was somewhere between 8 and 11.5, meaning that the adsorbent was positively charged when the pH was lower than the pH value of the IEP. The $Mo_7O_{24}^{6-}$ complexes are the dominant molybdenum chemical species at a pH range of 2 ~ 5 and the major species is MoO_4^{2-} at pH greater than 5 (Figure S3), when molybdenum concentration is 5 mg/mL [21]. The negatively charged molybdenum species in an acidic and neutral environment are beneficial for the adsorption on the positively charged UiO-66 (Ce). Fig. 3 (b) shows the effect of pH on the adsorption capacity of UiO-66 (Ce). The molybdenum uptake of UiO-66 (Ce) decreased gradually from 400 to 250 mg/g with increasing pH from 2 to 5, reaching eventually 220 mg/g at pH 8. This trend is consistent with the zeta potential of UiO-66 (Ce), suggesting that electrostatic attraction plays a key role in molybdenum adsorption. However, the adsorption capacity of UiO-66 (Ce) is still 182 mg/g when the zeta potential of the adsorbent was negative, indicating that electrostatic attraction was not the only interaction mechanism involved in the molybdenum adsorption.

3.2.2. Adsorption kinetics

Batch experiments were carried out to investigate the molybdenum adsorption isotherms and adsorption kinetics of UiO-66 (Ce). The molybdenum adsorption uptake was investigated at pH 3 for different incubation times, as shown in Fig. 4 (a). UiO-66 (Ce) showed an initial rapid molybdenum adsorption uptake, reaching 80% of the equilibrium value after 30 min for all studied concentrations. This fast adsorption kinetics could be due to the existence of many available sites on the external surface, which prompts molybdenum ions to diffuse into the adsorption sites [22]. The uptake was more than 90% of the equilibrium value after 1.5 h and reached saturation after 3 h, due to the diffusion of

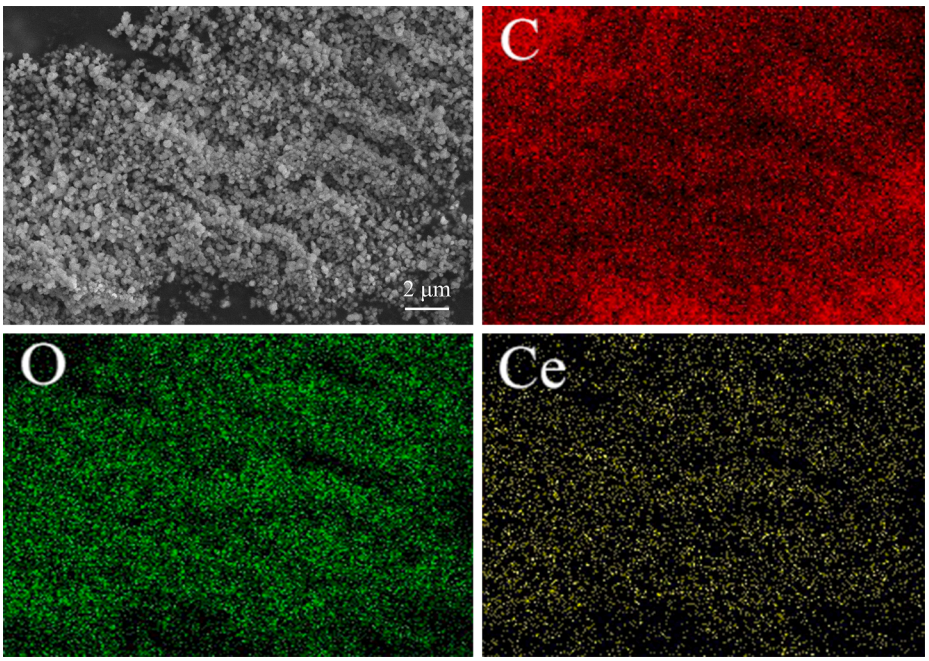

Fig. 1. SEM images and EDS mapping of UiO-66 (Ce) before molybdenum adsorption (b) C, (c) O and (d) Ce.

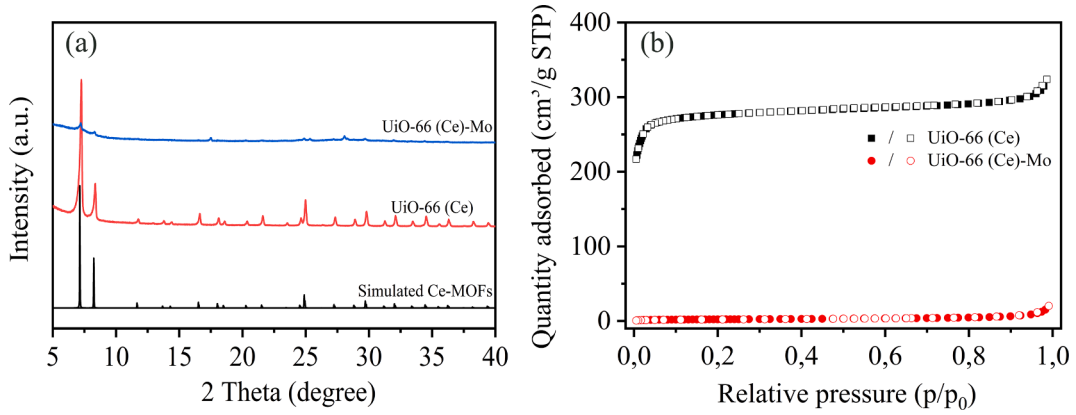

Fig. 2. (a) XRD patterns and (b) N2 adsorption–desorption isotherms of UiO-66 (Ce) before and after molybdenum adsorption at pH 3 in equilibrium concentration.

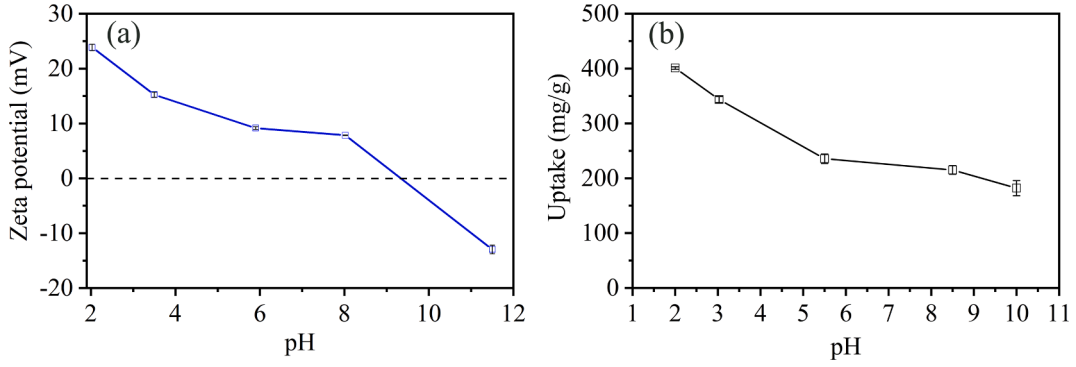

Fig. 3. Effect of pH on (a) zeta potential and (b) uptake of UiO-66 (Ce), the initial Mo concentration of 5 mg/mL.

molybdenum species into the inner pores of UiO-66 (Ce). Moreover, the equilibrium uptake of UiO-66 (Ce) increased when increasing the concentration and then remained stable when the initial molybdenum concentration was 10 mg/mL, suggesting that the molybdenum adsorption is closed to reach saturation. To further characterize the adsorption kinetics, the pseudo-first-order and pseudo-second-order kinetic models were applied to fit the adsorption kinetics. The fitting results of these models are displayed in Figure S4 and Table S1. These results indicated that the adsorption process was better described by the pseudo-second-order model, which according to the model indicated

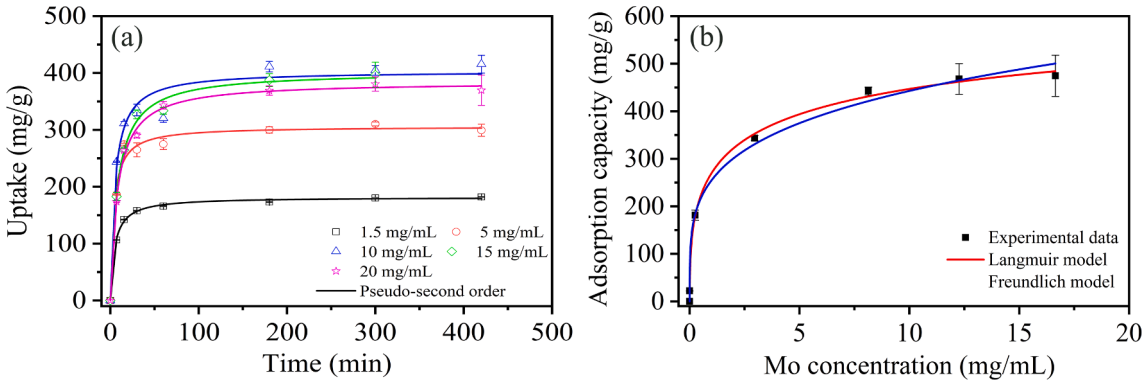

Fig. 4. Adsorption (a) kinetics non-linearly fitted by the pseudo-second-order model and (b) isotherms of UiO-66 (Ce) non-linearly fitted by the Langmuir and Freundlich models.

that the adsorption rate was dominated by chemical interaction [23]. In addition, the intraparticle diffusion model was employed to better understand the adsorption process. As shown in Figure S5 and Table S2, it can be observed that the first stage has a fast adsorption rate on the surface or adsorption sites of UiO-66 (Ce). In contrast, molybdenum species diffuse into inner pores showing a slower adsorption rate.

3.2.3. Adsorption isotherms

Fig. 4 (b) shows the Mo adsorption isotherm on UiO-66 (Ce) obtained by the varying initial molybdenum concentration from 0.1 to 20 mg/mL at pH 3. The adsorption uptake of the adsorbent increased abruptly at low concentrations, reaching a capacity of approximately ~ 350 mg/g at 5 mg/mL, which was more than 80% of the maximum adsorption capacity. Eventually, a plateau of around 475 mg/g, which is consistent with the results of the adsorption kinetics, was achieved. To further understand the molybdenum adsorption process, the Langmuir model and Freundlich models were employed to fit the experimental data. The non-linear fit results and calculated parameters are displayed in Table S3. The Langmuir model (R^2 = 0.997) can fit the experimental data better than the Freundlich model. The maximum adsorption capacity calculated by the Langmuir model was 485 mg/g, which is much higher when compared to that of UiO-66 (Zr) in our previous work [14]. Although the UiO-66 (Ce) has the same crystal structure as UiO-66 (Zr) and has a relatively lower surface area, the Ce-based MOF displayed a much higher molybdenum adsorption capacity, which is probably related to the inherent characteristics of cerium and will be discussed in the adsorption mechanism part of this paper. Moreover, this material exhibited the highest molybdenum adsorption capacity reported so far (Table S4).

3.3. Adsorption mechanism

XRD was utilized to analyse the structure of the UiO-66 (Ce) after adsorption (Fig. 2 (a)). The XRD analysis showed that all diffraction peaks still matched well with the sample before adsorption, which indicated that Ce-MOF-Mo kept its crystalline structure upon molybdenum adsorption. However, all diffraction peaks decreased in intensity after molybdenum adsorption, which was attributed to the trapped molybdenum species, causing the diminished X-ray contrast [24,25]. The N_2 adsorption–desorption experiment of the Ce-MOF-Mo was also carried out after adsorption (Fig. 2 (b)). The BET surface area and pore volumes were 8 m^2/g and 0.0009 cm^3/g, respectively. This dramatic decline in pore volume and surface area indicated that the molybdenum species completely filled the pores of the adsorbent. Furthermore, the EDS mapping (Figure S6) showed that the adsorbed molybdenum was distributed uniformly. (Table S5).

The Raman spectra of UiO-66 (Ce) before and after molybdenum adsorption at equilibrium concentration is presented in Fig. 5. The main

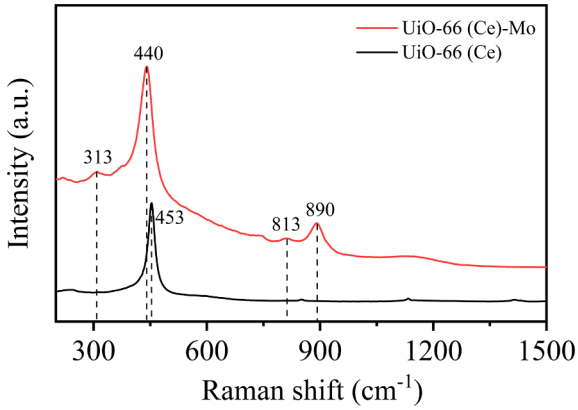

Fig. 5. Raman spectroscopy of UiO-66 (Ce) before and after molybdenum adsorption.

peak at 453 cm^{-1} is assigned to the symmetric stretching vibration of Ce-O bonds in metal clusters [26]. After molybdenum adsorption, the peak of UiO-66(Ce)-Mo at 440 cm^{-1} showed a blue-shift, which could be caused by the introduced molybdenum species or defects sites formed in the sample [27,28]. The broad and weak peaks at 313 cm^{-1} and 813 cm^{-1} were assigned to Mo = O bending vibrations and Mo-O-Mo antisymmetric stretches, respectively. A peak observed at 890 cm^{-1} was attributed to the Ce-O-Mo stretching vibration mode [29], which indicated that molybdenum species were anchored on the adsorbent by Ce-O-Mo coordination [30,31].

To further explore the adsorption mechanism, XPS spectra of UiO-66 (Ce) before and after adsorption were performed. The XPS spectra survey showed the existence of C, O and Ce elements in UiO-66 (Ce) before and after adsorption (Fig. 6 (a)). The new binding energy peaks for Ce-MOF-Mo at 228 ~ 240 eV and 410 ~ 420 eV were attributed to Mo 3d and Mo 3p spectra, respectively [32]. The lower binding energy peaks could be deconvoluted into two doublets at 232.0 eV and 235.1 eV (Fig. 6 (b)), which are assigned to Mo $3d_{5/2}$ and Mo $3d_{3/2}$, respectively, indicating the presence of Mo^{6+} [33]. The XPS Ce 3d spectrum of UiO-66 (Ce) before and after adsorption is shown in Fig. 6 (c). The whole spectrum could be deconvoluted into 8 peaks corresponding to two different valence states (Table S6). This is related to the electron configuration of Ce ($[Xe]4f^15d^16s^2$) and the low-lying nature of the empty 4f band, causing the formation of Ce^{4+} and partial reduction to Ce^{3+} [34,35]. The presence of Ce^{3+} cations could cause structural defects such as linker vacancies. These defects would induce the formation of Ce-OH groups [36–38], which are favourable for molybdenum adsorption. In addition, the shift of binding energy to a lower value indicates that the electron density of the Ce atoms increased after

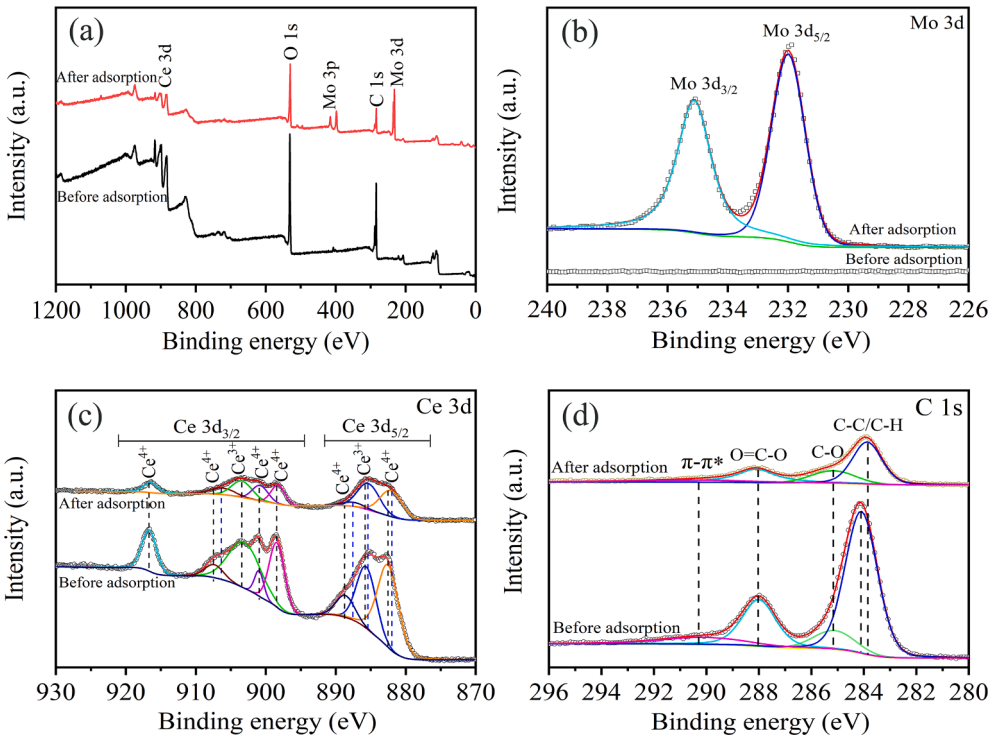

Fig. 6. (a) XPS survey spectrum, high-resolution XPS spectra of (b) Mo 3d, (c) Ce 3d and (4) C 1 s.

adsorption, which was probably due to the formation of Mo-O-Ce coordination bonds [39], matching with the observations of the Raman analysis. Fig. 6 (d) shows the C 1 s spectra of UiO-66 (Ce) before and after molybdenum adsorption. The C 1 s spectra could be deconvoluted into four peaks, which were assigned to π-π*, O = C-O, C-O and C-C/C-H (Table S7) [40]. After adsorption, the negative shift by 0.23 eV suggests a strong chemical interaction between C-C/C-H and molybdenum species via hydrogen bonds. The satellite peak at 290.1 eV was determined to be the π-π* component and its percentage decreased from 6.16% to 2.15% after molybdenum adsorption, suggesting the π-anions interaction between adsorbent and molybdenum species. Fig. S7 shows the UV absorbance spectra of UiO-66 (Ce). A peak was detected at 240 nm, which was ascribed to the π-π* transitions [40,41]. However, this peak disappeared after molybdenum adsorption, indicating that the π-π* component reacted with the molybdenum species, which is consistent with the C 1 s XPS results. Based on the above analysis, the interaction between the adsorbent and Mo species is governed by electrostatic attraction, hydrogen bonds formation, Mo-O-Ce coordination and π-anions.

3.4. Radiation stability of UiO-66 (Ce)

To further evaluate the adsorption performance of UiO-66 (Ce) as adsorbent for the ^{99}Mo/^{99m}Tc generator, adsorption experiments involving ^{99}Mo were carried out. The results showed that the adsorption capacities of the adsorbent were 11 mg/g, 184 mg/g and 304 mg/g, respectively, when the initial Mo concentrations were 0.1 mg/mL, 1.5 mg/mL and 5 mg/mL. This adsorption uptake was consistent with the adsorption capacity using the non-radioactive Mo solution. Moreover, the crystal structure of the adsorbent after adsorption was characterized by XRD (Fig. 7 (a)) and they all showed the same diffraction peaks as the original material, suggesting that the crystal structure of the adsorbent was not affected after ^{99}Mo adsorption. In addition, the radiation stability of UiO-66 (Ce) is an essential characteristic for its use in the ^{99}Mo/^{99m}Tc generator. Fig. 7 (b) shows the XRD patterns of UiO-66 (Ce) after exposure to different doses of gamma-ray originating from a Co-60 source. It can be confirmed that this adsorbent kept its good crystallinity after 550 kGy gamma irradiation, exhibiting an outstanding radiation resistance.

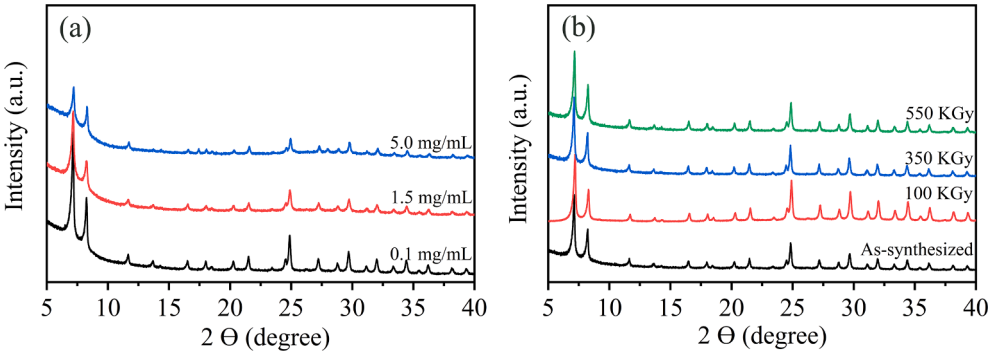

Fig. 7. XRD patterns of UiO-66 (Ce) (a) after 99Mo adsorption at pH 3 for 20 h and (b) after exposure to gamma-ray irradiation.

3.5. Performance of UiO-66 (Ce) as adsorbent in $^{99}Mo/^{99m}Tc$ generator

A $^{99}Mo/^{99m}Tc$ generator was packed using UiO-66 (Ce) particles as column bed. After loading ^{99}Mo, the adsorption capacity of the UiO-66 (Ce) generator was determined to be 297 mg/mL, which was consistent with the previous results when non-radioactive molybdenum was applied. Then the column was rinsed with 0.9% saline solution to remove the loosely absorbed molybdenum ions. The practical adsorption capacity of UiO-66 (Ce) was calculated to be 246 mg/g, which was close to the uptake value in the pH range of 5 to 8 (as shown in Fig. 3 (b)). Afterwards, the column was eluted daily using 0.9% saline solution (pH = 6) for two consecutive weeks. The elution yield and cumulative yield curve of ^{99m}Tc as a function of the volume of the eluted saline solution are shown in Fig. 8. It was observed that the elution yield of ^{99m}Tc decreased sharply with the increasing volume of the saline solution. More than 99% of ^{99m}Tc could be collected after passing 6 mL of saline solution through the generator. In Table 1, the elution efficiency and the ^{99}Mo and Ce breakthrough of the $^{99}Mo/^{99m}Tc$ generator are displayed. It can be seen that the elution yield of ^{99m}Tc was 92 ± 3% and remained around that value for two weeks. There is about 0.2%~0.3% of ^{99}Mo contamination in each elution fraction, which is slightly higher than the requirement (<0.1%) defined by the International Pharmacopoeia [42]. The Ce breakthrough in all elution fractions was determined to be around 1 ppm.

The total activity of many commercial generators is about 2 Ci when 2 g of adsorbent is typically used. Alternative production methods to ^{235}U fission can provide ^{99}Mo with specific activity in the range of 1–10 Ci/g [43]. Assuming a generator fabricated with 2 g of UiO-66 (Ce) and 6 Ci/g of specific activity of ^{99}Mo, this adsorbent should be able to deliver 3 Ci of ^{99}Mo, when ~ 52% of the maximum adsorption capacity (250 mg/g) was applied here. In addition, the column experiment was repeated and the results are shown in Table S8. About 92% of ^{99m}Tc elution yield can be achieved, which corresponds with previous results, showing good repeatability. The above results indicated that UiO-66 (Ce) exhibited great potential as adsorbent for $^{99}Mo/^{99m}Tc$ generator utilizing low specific activity ^{99}Mo, providing new exciting opportunities for production using more production facilities worldwide.

4. Conclusions

UiO-66 (Ce) was synthesized successfully and utilized as adsorbent for $^{99}Mo/^{99m}Tc$ generator. The maximum adsorption capacity of the adsorbent was 475 mg/g and the adsorption reached equilibrium within 3 h. The positive charge of the adsorbent was favourable for molybdenum adsorption by electrostatic attraction. The XPS results confirmed the existence of Ce^{3+}/Ce^{4+} i.e. two chemical valences, causing linker defects and the formation of extra hydroxyl groups, which were beneficial for molybdenum adsorption via coordination interaction, π-anions and hydrogen bonds. Moreover, the adsorption performance of UiO-66 (Ce) using radioactive ^{99}Mo solution verified its good adsorption behaviour and radiation stability. The column results showed that about 92 ± 3% elution efficiency of ^{99m}Tc and low cerium breakthrough could be achieved for two-week elution. The excellent performance of the developed $^{99}Mo/^{99m}Tc$ generator reveals that UiO-66 (Ce) is a great adsorbent candidate for applications using low specific activity ^{99}Mo.

CRediT authorship contribution statement

Chao Ma: Conceptualization, Data curation, Formal analysis, Methodology, Validation, Writing – original draft. **Hubert T. Wolterbeek:** Supervision. **Antonia G. Denkova:** Supervision, Project administration, Writing – review & editing. **Pablo Serra Crespo:** Supervision, Funding acquisition, Conceptualization, Project administration, Writing – review & editing.

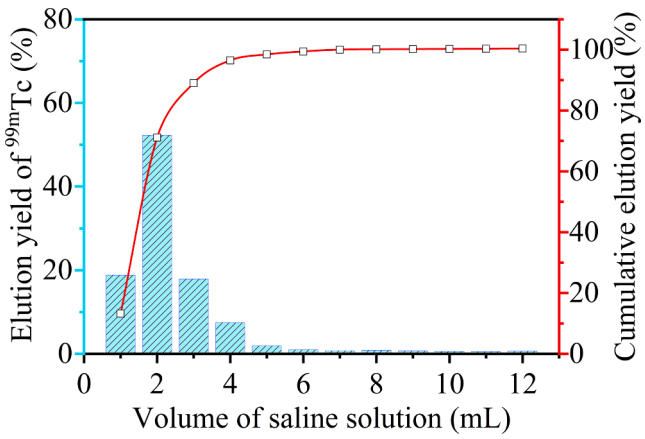

Fig. 8. Elution yield of 99mTc of the 99Mo/99mTc generator using saline solution (pH = 6).

Table 1
Elution performance of UiO-66 (Ce) in the $^{99}Mo/^{99m}Tc$ generator over two weeks.

Elution No.	Time of ingrowth (h)	Elution efficiency (%)	^{99}Mo breakthrough (%)	Ce breakthrough (ppm)
1	24	88.8	0.36	1.21
2	72	87.7	0.21	0.92
3	24	91.2	0.28	0.46
4	24	91.0	0.24	0.99
5	24	93.6	0.30	0.98
6	24	90.2	0.33	0.96
7	68	88.6	0.20	0.27
8	24	91.7	0.29	0.96
9	23	93.5	0.19	0.92
10	24	96.9	0.24	0.53
11	24	95.9	0.29	0.93
12	72	96.6	0.09	0.81

Declaration of Competing Interest

The authors declare that they have no known competing financial interests or personal relationships that could have appeared to influence the work reported in this paper.

Acknowledgments

The authors are grateful to the China Scholarship Council (Grant No. 201807040061). We appreciate Willy Rook for her help with the N_2 adsorption measurements. We gratefully acknowledge Bart Boshuizen for the XPS measurement. We also would like to thank Katalin Gmeling from the Institute for Energy Security and Environmental Safety Centre for Energy Research, Hungary to supply the radioactive molybdenum.

Appendix A. Supplementary data

Supplementary data to this article can be found online at https://doi.org/10.1016/j.seppur.2022.121218.

References

[1] M.R. Pillai, A. Dash, F.F. Knapp, Sustained availability of ^{99m}Tc: possible paths forward, J. Nucl. Med. 54 (2013) 313–323, https://doi.org/10.2967/jnumed.112.110338.
[2] A. Dash, R. Chakravarty, Pivotal role of separation chemistry in the development of radionuclide generators to meet clinical demands, RSC Adv. 4 (81) (2014) 42779–42803, https://doi.org/10.1039/c4ra07218a.
[3] R. Chakravarty, R. Ram, R. Mishra, D. Sen, S. Mazumder, M.R.A. Pillai, A. Dash, Mesoporous Alumina (MA) Based Double Column Approach for Development of a

Clinical Scale $^{99}Mo/^{99m}Tc$ Generator Using (n, γ)^{9}9Mo: An Enticing Application of Nanomaterial, Ind. Eng. Chem. Res. 52 (33) (2013) 11673–11684, https://doi.org/10.1021/ie401042n.
[4] H. Naik, S.V. Suryanarayana, K.C. Jagadeesan, S.V. Thakare, P.V. Joshi, V. T. Nimje, K.C. Mittal, A. Goswami, V. Venugopal, S. Kailas, An alternative route for the preparation of the medical isotope ^{99}Mo from the ^{238}U(γ, f) and ^{100}Mo(γ, n) reactions, J. Radioanal. Nucl. Chem. 295 (1) (2012) 807–816, https://doi.org/10.1007/s10967-012-1958-9.
[5] J. Wang, R. Gao, Q. Huang, X. Yin, M. Lin, S. Cao, D. Chen, F. Fan, X. Wu, Z. Qin, Z. Guo, J. Bai, J. Chu, W. Tian, C. Tan, B. Li, N. Cheng, Z. Jia, Practicality of hierarchically macro/mesoporous γ-Al_2O_3 as a promising sorbent in the preparation of low specific activity $^{99}Mo/^{99m}Tc$ generator, Appl. Radiat. Isot. 178 (2021), 109986, https://doi.org/10.1016/j.apradiso.2021.109986.
[6] I. Saptiama, Y.V. Kaneti, Y. Suzuki, Y. Suzuki, K. Tsuchiya, T. Sakae, K. Takai, N. Fukumitsu, Z.A. Alothman, M.S.A. Hossain, K. Ariga, Y. Yamauchi, Mesoporous Alumina as an Effective Adsorbent for Molybdenum (Mo) toward Instant Production of Radioisotope for Medical Use, Bull. Chem. Soc. Jpn. 90 (10) (2017) 1174–1179, https://doi.org/10.1246/bcsj.20170184.
[7] M. Tanase, K. Tatenuma, K. Ishikawa, K. Kurosawa, M. Nishino, Y. Hasegawa, A ^{99m}Tc generator using a new inorganic polymer adsorbent for (n, γ) ^{9}9Mo, Appl. Radiat. Isot. 48 (5) (1997) 607–611, https://doi.org/10.1016/s0969-8043(96)00320-x.
[8] S. Hasan, M.A. Prelas, Molybdenum-99 production pathways and the sorbents for $^{99}Mo/^{99m}Tc$ generator systems using (n, γ) ^{9}9Mo: a review, SN Appl. Sci. 2 (11) (2020) 1–28, https://doi.org/10.1007/s42452-020-03524-1.
[9] A. Dash, R. Chakravarty, Nanomaterial-Based Adsorbent: Promises, Opportunities, and Challenges to Develop Column Chromatography Radionuclide Generators for Nuclear Medicine, Sep. Purif. Rev. 46 (2) (2016) 91–107, https://doi.org/10.1080/15422119.2016.1205089.
[10] J. Canivet, A. Fateeva, Y. Guo, B. Coasne, D. Farrusseng, Water adsorption in MOFs: fundamentals and applications, Chem. Soc. Rev. 43 (16) (2014) 5594–5617, https://doi.org/10.1039/c4cs00078a.
[11] N. Stock, S. Biswas, Synthesis of metal-organic frameworks (MOFs): routes to various MOF topologies, morphologies, and composites, Chem. Rev. 112 (2) (2012) 933–969, https://doi.org/10.1021/cr200304e.
[12] M. Kandiah, M.H. Nilsen, S. Usseglio, S. Jakobsen, U. Olsbye, M. Tilset, C. Larabi, E.A. Quadrelli, F. Bonino, K.P. Lillerud, Synthesis and Stability of Tagged UiO-66 Zr-MOFs, Chem. Mater. 22 (24) (2010) 6632–6640, https://doi.org/10.1021/cm102601v.
[13] F. Ahmadijokani, R. Mohammadkhani, S. Ahmadipouya, A. Shokrgozar, M. Rezakazemi, H. Molavi, T.M. Aminabhavi, M. Arjmand, Superior chemical stability of UiO-66 metal-organic frameworks (MOFs) for selective dye adsorption, Chem. Eng. J. 399 (2020), 125346, https://doi.org/10.1016/j.cej.2020.125346.
[14] C. Ma, A. Vasileiadis, H.T. Wolterbeek, A.G. Denkova, P. Serra Crespo, Adsorption of molybdenum on Zr-based MOFs for potential application in the $^{99}Mo/^{99m}Tc$ generator, Appl. Surf. Sci., 572 (2022), pp. 151340, 10.1016/j.apsusc.2021.151340.
[15] J. He, Y. Xu, Z. Xiong, B. Lai, Y. Sun, Y. Yang, L. Yang, The enhanced removal of phosphate by structural defects and competitive fluoride adsorption on cerium-based adsorbent, Chemosphere 256 (2020), 127056, https://doi.org/10.1016/j.chemosphere.2020.127056.
[16] M. Lammert, M.T. Wharmby, S. Smolders, B. Bueken, A. Lieb, K.A. Lomachenko, D. D. Vos, N. Stock, Cerium-based metal organic frameworks with UiO-66 architecture: synthesis, properties and redox catalytic activity, Chem. Commun. 51 (63) (2015) 12578–12581, https://doi.org/10.1039/c5cc02606g.
[17] Z. Hu, Y. Wang, D. Zhao, The chemistry and applications of hafnium and cerium (iv) metal-organic frameworks, Chem. Soc. Rev. 50 (7) (2021) 4629–4683, https://doi.org/10.1039/d0cs00920b.
[18] J. Yang, K. Li, C. Li, J. Gu, Intrinsic Apyrase-Like Activity of Cerium-Based Metal-Organic Frameworks (MOFs): Dephosphorylation of Adenosine Tri- and Diphosphate, Angew. Chem. Int. Ed. 59 (51) (2020) 22952–22956, https://doi.org/10.1002/anie.202008259.
[19] Y. Zhang, X. Zeng, X. Jiang, H. Chen, Z. Long, Ce-based UiO-66 metal-organic frameworks as a new redox catalyst for atomic spectrometric determination of Se (VI) and colorimetric sensing of Hg(II), Microchem. J. 149 (2019), 103967, https://doi.org/10.1016/j.microc.2019.103967.
[20] L. Cifuentes, C. Ramírez, G. Crisóstomo, J.M. Casas, Separation of Molybdenum Species by Electrodialysis, Chem. Eng. Commun. 198 (6) (2011) 805–814, https://doi.org/10.1080/00986445.2011.534015.
[21] L. Man-Seung, S. Seong-Ho, L. Myung-Ho, Ionic Equilibria and Ion Exchange of Molybdenum(VI) from Strong Acid Solution, Bulletin Korean Chem. Soc. 32 (2011) 3687–3691, https://doi.org/10.5012/bkcs.2011.32.10.3687.
[22] J. Wu, J. Zhou, S. Zhang, A. Alsaedi, T. Hayat, J. Li, Y. Song, Efficient removal of metal contaminants by EDTA modified MOF from aqueous solutions, J. Colloid. Interface Sci. 555 (2019) 403–412, https://doi.org/10.1016/j.jcis.2019.07.108.
[23] W. Tan, T. Chen, W.R. Liu, F.G. Ye, S.L. Zhao, Design and fabrication of boric acid functionalized hierarchical porous metal-organic frameworks for specific removal of cis-diol-containing compounds from aqueous solution, Appl. Surf. Sci. 535 (2021), 147714, https://doi.org/10.1016/j.apsusc.2020.147714.
[24] J.L. Gu, J.L. Shi, G.J. You, L.M. Xiong, S.X. Qian, Z.L. Hua, H.R. Chen, Incorporation of highly dispersed gold nanoparticles into the pore channels of mesoporous silica thin films and their ultrafast nonlinear optical response, Adv. Mater. 17 (5) (2005) 557–560, https://doi.org/10.1002/adma.200401085.
[25] X. Zhu, B. Li, J. Yang, Y. Li, W. Zhao, J. Shi, J. Gu, Effective adsorption and enhanced removal of organophosphorus pesticides from aqueous solution by Zr-based MOFs of UiO-67, ACS Appl. Mater. Interfaces 7 (1) (2015) 223–231, https://doi.org/10.1021/am5059074.
[26] E. Villa-Aleman, A.L. Houk, D.D. Dick, S.E.H. Murph, Hyper-Raman spectroscopy of CeO_2, J. Raman Spectrosc. 51 (7) (2020) 1260–1263, https://doi.org/10.1002/jrs.5886.
[27] L. Wang, J. Zhang, G. Wang, W. Zhang, C. Wang, C. Bian, F.S. Xiao, Selective hydrogenolysis of carbon-oxygen bonds with formic acid over a Au-Pt alloy catalyst, Chem. Commun. 53 (18) (2017) 2681–2684, https://doi.org/10.1039/c6cc09599b.
[28] F. Wang, S. He, H. Chen, B. Wang, L. Zheng, M. Wei, D.G. Evans, X. Duan, Active Site Dependent Reaction Mechanism over Ru/CeO_2 Catalyst toward CO_2 Methanation, J. Am. Chem. Soc. 138 (19) (2016) 6298–6305, https://doi.org/10.1021/jacs.6b02762.
[29] W.X. Kuang, Y.N. Fan, K.D. Chen, Y. Chen, Partial oxidation of toluene over ultrafine mixed Mo-based oxide particles, J. Catal. 186 (2) (1999) 310–317, https://doi.org/10.1006/jcat.1999.2559.
[30] F. Chandoul, A. Boukhachem, F. Hosni, H. Moussa, M.S. Fayache, M. Amlouk, R. Schneider, Change of the properties of nanostructured MoO_3 thin films using gamma-ray irradiation, Ceram. Int. 44 (11) (2018) 12483–12490, https://doi.org/10.1016/j.ceramint.2018.04.040.
[31] H. Jeziorowski, H. Knozinger, Raman and Ultraviolet Spectroscopic Characterization of Molybdena on Alumina Catalysts, J. Phys. Chem. 83 (9) (1979) 1166–1173, https://doi.org/10.1021/j100472a012.
[32] G.D. Khattak, M.A. Salim, A.S. AlHarthi, D.J. Thompson, L.E. Wenger, Structure of molybdenum-phosphate glasses by X-ray photoelectron spectroscopy (XPS), J. Non-Cryst. Solids 212 (2–3) (1997) 180–191, https://doi.org/10.1016/S0022-3093(97)00023-9.
[33] G. Tai, T. Zeng, J. Yu, J. Zhou, Y. You, X. Wang, H. Wu, X. Sun, T. Hu, W. Guo, Fast and large-area growth of uniform MoS_2 monolayers on molybdenum foils, Nanoscale 8 (4) (2016) 2234–2241, https://doi.org/10.1039/c5nr07226c.
[34] F. Esch, S. Fabris, L. Zhou, T. Montini, C. Africh, P. Fornasiero, G. Comelli, R. Rosei, Electron localization determines defect formation on ceria substrates, Science 309 (5735) (2005) 752–755, https://doi.org/10.1126/science.1111568.
[35] X.P. Wu, L. Gagliardi, D.G. Truhlar, Cerium Metal-Organic Framework for Photocatalysis, J. Am. Chem. Soc. 140 (25) (2018) 7904–7912, https://doi.org/10.1021/jacs.8b03613.
[36] H. Giang, T. Nguyen, N.M. Schweitzer, C.-Y. Chang, T.L. Drake, M.C. So, P.C. Stair, O.K. Farha, J.T. Hupp, S.T. Nguyen, Vanadium-Node-Functionalized UiO-66: A Thermally Stable MOF-Supported Catalyst for the Gas-Phase Oxidative Dehydrogenation of Cyclohexene, ACS Catal. 4 (8) (2014) 2496–2500, https://doi.org/10.1021/cs5001448.
[37] M. Wen, Y. Kuwahara, K. Mori, D. Zhang, H. Li, H. Yamashita, Synthesis of Ce ions doped metal–organic framework for promoting catalytic H_2 production from ammonia borane under visible light irradiation, J. Mater. Chem. A 3 (27) (2015) 14134–14141, https://doi.org/10.1039/c5ta02320c.
[38] F. Nouar, M.I. Breeze, B.C. Campo, A. Vimont, G. Clet, M. Daturi, T. Devic, R. I. Walton, C. Serre, Tuning the properties of the UiO-66 metal organic framework by Ce substitution, Chem. Commun. 51 (77) (2015) 14458–14461, https://doi.org/10.1039/c5cc05072c.
[39] Z.J. Lin, H.Q. Zheng, Y.N. Zeng, Y.L. Wang, J. Chen, G.J. Cao, J.F. Gu, B.L. Chen, Effective and selective adsorption of organoarsenic acids from water over a Zr-based metal-organic framework, Chem. Eng. J. 378 (2019), 122196, https://doi.org/10.1016/j.cej.2019.122196.
[40] H.N. Abdelhamid, G.A. Mahmoud, W. Sharmouk, A cerium-based MOFzyme with multi-enzyme-like activity for the disruption and inhibition of fungal recolonization, J. Mater. Chem. B 8 (33) (2020) 7548–7556, https://doi.org/10.1039/d0tb00894j.
[41] J. He, J. Wang, Y. Chen, J. Zhang, D. Duan, Y. Wang, Z. Yan, A dye-sensitized Pt@UiO-66(Zr) metal-organic framework for visible-light photocatalytic hydrogen production, Chem. Commun. 50 (53) (2014) 7063–7066, https://doi.org/10.1039/c4cc01086h.
[42] Sodium Pertechnetate (^{99m}Tc) Injection (Non-Fission): Final text for addition to the International Pharmacopoeia, World Health Organization Document, 2009.
[43] V.S. Le, ^{99m}Tc generator development: up-to-date ^{99m}Tc recovery technologies for increasing the effectiveness of ^{99}Mo utilisation, Sci. Technol. Nucl. Install. 2014 (2014) 1–41, https://doi.org/10.1155/2014/345252.